

*Keywords: FEM, Finite Element Method, dynamic analysis, ductile damage, Abaqus*

*Kuba ROŚLANIEC* [0000-0002-4093-1702]\*

# **ANALYSIS OF THE EFFECT OF PROJECTILE IMPACT ANGLE ON THE PUNCTURE OF A STEEL PLATE USING THE FINITE ELEMENT METHOD IN ABAQUS SOFTWARE**

## **Abstract**

*This paper deals with the punctureability of a steel plate by a projectile at different angles of attack. The effect of the projectile angle on the force required to penetrate a plate made of A36 steel is presented using Finite Element Method calculation software. Using Abaqus software, a dynamic model of a projectile striking a plate was modelled and the force required to penetrate a 5 mm thick steel plate was presented. The introduction gives an overview of the genesis of the topic and a brief historical background. The chapter on numerical analysis presents the numerical model used and how the simulation was modelled. In the conclusions, a summary of the results was formulated and conclusions were drawn regarding the observations and insights of the analysis. The force required to penetrate the plate was observed to increase with increasing projectile angle of attack and it was found that, as the angle of the plate increased, the force required to penetrate increased.*

## **1. INTRODUCTION**

The problem of steel plate penetrability became widespread when the first tank appeared on the battlefield, the British Mark I. The concept of armoured weapons was then born, and with it the idea of destroying them (Fletcher, 2004).

The ability to penetrate armour depends on the properties of the armour, the properties of the projectile (material from which it was made, design, type of detonator) and the velocity, angle of attack of the projectile and the shape of its nose. In the article "Ballistic resistance of 2024 aluminium plates against hemispherical, spherical and blunt nose projectiles", it was observed that the lowest permeability is characteristic of projectiles with a spherical nose in comparison with projectiles with a hemispherical and flat nose. At low velocities, flat nose projectiles had the highest global energy (Senthil et al, 2018).

---

\* Lublin University of Technology, Poland

In order to improve the vehicle's resistance to bullet penetration, the thickness of the armour was increased, resulting in an increase in weight, and a deterioration in the vehicle's mobility and manoeuvrability. For this reason, research began into more puncture-resistant materials, and due to the impossibility of carrying out non-destructive tests, experiments were carried out by shooting at armour plates with various types of weapons. Figure 1 shows a ballistic plate which was tested on a firing range (Torecki, 1982). In the course of experimental research, extended by the achievements of modern technology and computer simulation medotypes, it was observed that, in the case of thin plates (in relation to the diameter of the projectile), when the local deformation was twice as large as the diameter of the plate, almost no global deformation was registered, in the case of thicker plates this phenomenon is not observed. With increasing plate thickness and impact velocity, an increase in projectile deformation is observed. It was also found that the perforation time of the plate is relatively constant for different plate thicknesses at impact velocities close to the limit velocity required to perforate the material. In the case of not piercing the metal plate, exceeding the ballistic limit, projectile cracking was observed causing minor damage to the plate (Børvik et al, 2003).

Ballistic tests showed that the highest resistance to penetration by conventional armour-piercing bullets characterised the plates made steels with a significant content of alloying elements, such as Mo-molybdenum (eliminates brittleness), Cr-chromium (increases hardness), Ni-nickel (increases yield strength, which is an important prerequisite for strength, in conventional bullets). Due to the complexity of the production process and the high price of alloying elements, armour plates made of alloy steels were significantly more expensive than their non-alloy counterparts. In the 1930s, the Soviet Union commissioned the Kharkov Steam Engine Factory to develop a universal tank. Mikhail Koshkin's team observed during the testing of the prototype BT-SV tank, as illustrated in the Figure 3, the beneficial effect of setting the armour plates at an angle (Michulec & Zientarzewski, 2006; Flis & Sperski, 2012).



**Fig. 1.** View of a section of an 80 mm thick plate under test firing (Aufmann, 2020)

As the angle of inclination of the armour increases, the effective thickness of the armour (i.e., the thickness of the armour through which the bullet must penetrate to pierce the armour) is greater. The dependence of the effective armour thickness on the angle of inclination is shown in Figure 2. Furthermore, compared to a projectile striking a plate positioned perpendicular to the angle of attack of the projectile, where the entire kinetic energy of the projectile is transferred to the armoured plate, there is a partial dissipation of this energy, and there is an increased chance of the projectile rebounding, sliding off the vehicle plate, the so-called ricochet (Torecki, 1982; Michulec & Zientarzewski, 2006). When the projectile hits the plate, the kinetic energy of the system decreases, it is converted into work needed to overcome the force of resistance and work of deformation. It has also been observed that the most favourable situation is that the structure of the armour plate is not damaged by the projectile, which results in the ballistic protection of the plate not being affected. It should be borne in mind that in certain situations increasing the angle of inclination of the plate is not a fully effective method of protection, due to the possibility of the aforementioned ricochets causing damage to other people or other vehicles (Nieoczym & Drozd, 2021).

In this paper, a numerical analysis is carried out for a homogeneous steel plate that has constant physical and chemical properties throughout its cross-section. These plates are the least advanced type of steel plates used in military facilities and vehicles, however, due to their relatively low price, and easy manufacturing process, they were widely used in the 20th century (Michulec & Zientarzewski, 2006; Flis & Sperski, 2012).

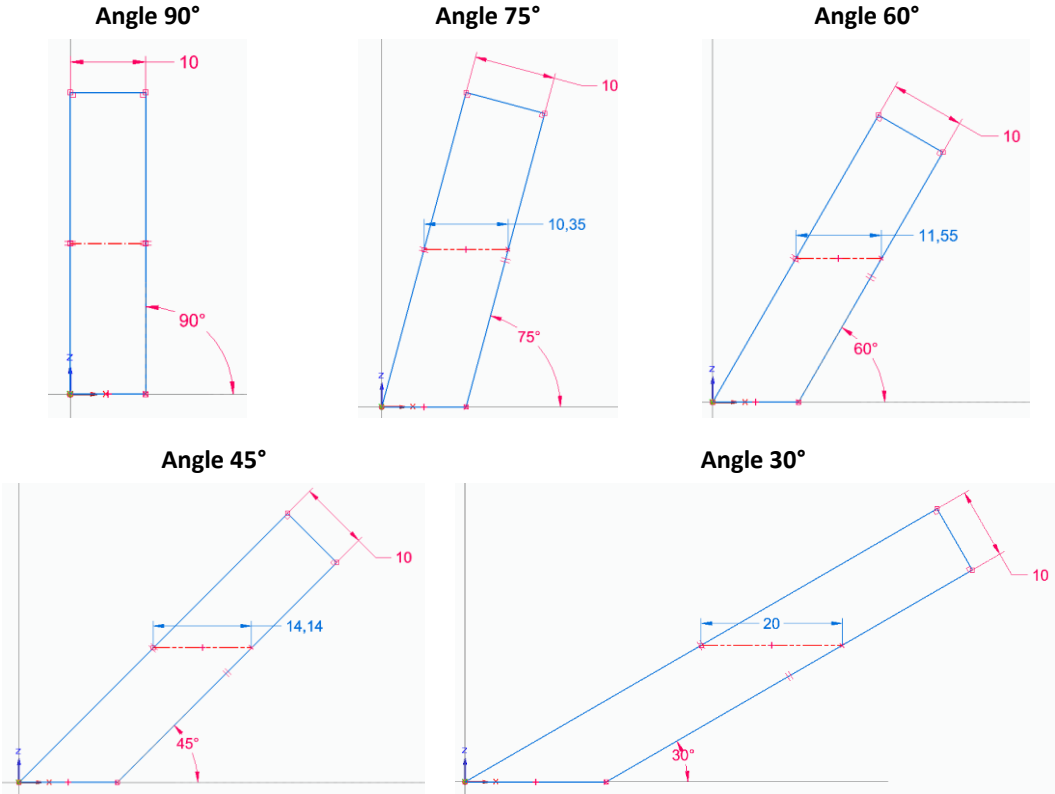


Fig. 2. Effect of armour plate inclination angle on effective armour thickness



**Fig. 3. View of a section of an 80 mm thick plate under test firing (Czołg lekki BT-SV-2 „Turtle”, n.d.)**

## **2. NUMERICAL ANALYSIS**

In the analytical method, Newton's laws are used to describe the motion of the material particles pierced by the projectile, this motion has the character of a plasticised movement of the material particles in three-dimensional space. This leads to the formulation of complex systems of molecular differential equations. Attempts to estimate by analytical means the simple case of armour piercing by a projectile have a lower accuracy than numerical analyses, as the level of complexity of the model increases, the inaccuracy of the analytical model increases. However, analytical methods can be used for preliminary assessment and analysis of the correctness of finite element calculations. In addition, computer simulation provides information about the deformations and stresses produced during the material puncture test (Budzyński, 2006; Wiśniewski & Żurowski, 2002)

The essence of the Finite Element Method (FEM) is the approximation of a continuous medium with an infinite number of degrees of freedom by using a discrete model with a finite number of degrees of freedom. The foundations of the Finite Element Method were published in a paper by Kirschhof in 1868. He proposed to replace the three-dimensional system a continuous spatial truss composed of cuboid elements. The revival of the above idea took place after the Second World War, thanks to Polish scientists – Professor Olgierd Zienkiewicz and Professor Janusz Przemieniecki. They tackled the problem of the excessive number of unknowns in equilibrium systems. Prof. Zienkiewicz is regarded as the creator and forerunner of the Finite Element Method and its applications in mechanics. The use of this method involves solving equations with thousands of unknowns (Bathe, 1996; Flis & Sperski, 2011).

The ductile damage initiation criterion was adopted to estimate the effect of projectile angle on plate penetrability. It is used to predict the onset and expansion of damage caused by nucleation, growth and coalescence of voids in ductile metals. The ductile damage initiation criterion was adopted to estimate the effect of projectile angle on plate penetrability.

It is used to predict the onset and expansion of damage caused by nucleation, growth and coalescence of voids in ductile metals. This model assumes that, the onset of plastic deformation is equivalent (is equivalent) to a function of stress triaxiality and strain rate (Simulia, 2017; Wagner, 2021).

$$\bar{\epsilon}_D^{pl} = d_0 e^{-c\mu} + d_1 e^{c\mu} \quad (1)$$

where:  $\bar{\epsilon}_D^{pl}$  – stress-strain rate triaxial function,

$\mu = \frac{-p}{q}$  – stress triaxiality function,

$p$  – pressure stress,

$q$  – mises equivalent stresses,

$c, d_0, d_1$  – aterial characteristics obtained from research and testing.

All equations included in the paper are taken from (Simulia, 2017).

The application of this computational model requires advanced research and testing, due to its significant cost, labour intensity and difficulty of implementation, the article refers to the results of other researchers. The material properties of the steel were obtained from tensile coupon tests as described in the experimental study: "More Details about Validation of Calibrated Parameters of Ductile Damage Model for A36 Steel Plates in Abaqus Software" (Tiwari, Iqbal & Gupta, 2018). The penetration simulations were carried out for a plate made of A36 steel. It is a high strength structural carbon steel used for hot rolled plates, shaped bars and universal profiles. It is characterised by good weldability to ASTM standards, an important feature in the manufacture of armoured vehicles (Steel Construction Manual, 1986).

**Tab. 1. Percentage chemical composition of A36 steel in ASTM standard (Steel Construction Manual, 1986)**

<b>C</b>	<b>Si</b>	<b>Mn*</b>	<b>S</b>	<b>P</b>	<b>Cu</b>
≤ 0.25	≤ 0.40	–	≤ 0.05	≤ 0.04	≥ 0.20

\*The manganese content is not regulated.

**Tab. 2. Physical and mechanical properties in analysis (Steel Construction Manual, 1986)**

<b>Tensile Strength, Ultimate</b>	550 MPa
<b>Plastic Strain</b>	0.2
<b>Tensile Strength, Yield</b>	250 MPa
<b>Modulus of Elasticity</b>	200 GPa
<b>Poissons Ratio</b>	0.26
<b>Shear Modulus</b>	79.3 GPa
<b>Density</b>	7.85 g/cm <sup>3</sup>

For damage, the Damage Evolution sub-option has been added to the material model. Fracture strain is an equivalent strain at damage initiation. Figure 4 shows the relationship between stress and strain that a material undergoes in during failure – a continuous line, while the dashed curve is the relationship in the absence of damage. The displacement value at failure corresponds to the product of the characteristic length of the elements and the strain at failure (Wagner, 2021; Askariani & Garivani, 2020).

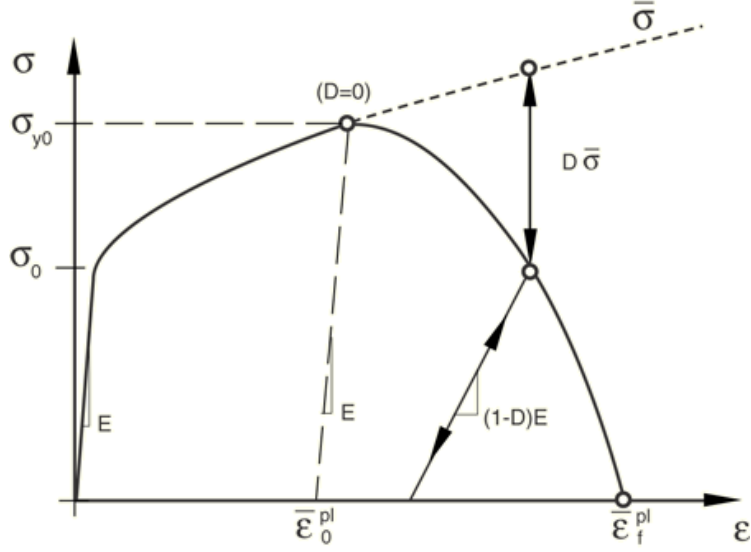


**Fig. 4. Stress-strain curve plot with advancing damage degradation (Simulia, 2017)**

The stress triaxiality is defined as ratio pressure stress  $-p$  and the mises equivalent stress  $-q$  (Simulia, 2017; Wagner, 2021).

$$\eta = \frac{-p}{q} \quad (2)$$

The strain rate is an equivalent plastic strain rate. The strain rate is the deformation, the deformation of a material over time, due to a load (Simulia, 2017; Wagner, 2021).

$$\epsilon(t) = \frac{L(t) - L_0}{L_0} \quad (3)$$

$$\dot{\epsilon} = \frac{d\epsilon}{dt} = \frac{d}{dt} \left( \frac{L(t) - L_0}{L_0} \right) = \frac{1}{L_0} \times \frac{dL(t)}{dt} = \frac{v(t)}{L_0} \quad (4)$$

Displacement damage evolution is defined as a function of the total, for cohesive elements or bulk elastic-plastic materials, displacement at the time of damage initiation. The value of the failure properties adopted are shown in Table 3 and Figure 4 (Wagner, 2021).

**Tab. 3. The Required values of Ductile Damage model for A36 steel plates (N, mm), (Askariani & Garivani, 2020).**

No.	Fracture Strain	Stress Triaxiality	Strain Rate	No.	Fracture Strain	Stress Triaxiality	Strain Rate
1	3.4285	0.01	1	20	2.3207	0.2	1
2	3.3587	0.02	1	21	2.2736	0.21	1
3	3.2903	0.03	1	22	2.2275	0.22	1
4	3.2233	0.04	1	23	2.1823	0.23	1
5	3.1577	0.05	1	24	2.1381	0.24	1
6	3.0934	0.06	1	25	2.0948	0.25	1
7	3.0305	0.07	1	26	1.8913	0.3	1
8	2.9688	0.08	1	27	1.5430	0.4	1
9	2.9084	0.09	1	28	1.2606	0.5	1
10	2.8493	0.1	1	29	1.0322	0.6	1
11	2.7913	0.11	1	30	0.8480	0.7	1
12	2.7346	0.12	1	31	0.7001	0.8	1
13	2.6790	0.13	1	32	0.5821	0.9	1
14	2.6246	0.14	1	33	0.4891	1	1
15	2.5712	0.15	1	34	0.4169	1.1	1
16	2.5190	0.16	1	35	0.3626	1.2	1
17	2.4679	0.17	1	36	0.3239	1.3	1
18	2.4178	0.18	1	37	0.2990	1.4	1
19	2.3687	0.19	1	38	0.2868	1.5	1

Displacement at Failure	
1	0.3

**Fig. 5. Damage Evolution suboption settings in the Ductile Damage material model for A36 steel plates (N, mm) (Tyutin, Botvinaa & Petersen, 2020)**

In this study, the numerical simulation was carried out in Abaqus software, dedicated to carrying out advanced simulations using the Finite Element Method. The computational model consists of two elements, the object of analysis being a steel plate made of A36 steel, shot through by a projectile at various angles of attack, with a constant velocity of  $V = 10000$  mm/s, along the Z axis relative to the reference system, in order to eliminate unfavourable projectile displacement, projectile movement in the X and Y planes is blocked. Steel plate restrained by locking the possibility of movement in the X, Y, Z plane on the lateral edge of the disc. The model of the shot-peened slab (a disc of 50 mm diameter and 5 mm thickness) was designed as a deformable solid object, with a Mesh type C3D8R (An 8-node linear brick, reduced integration, hourglass control), composed of 12100 finite elements. The slab was shot through at the following angles of attack:

- 90° (effective thickness -5 mm),
  - 75° (effective thickness -5.18 mm, increased thickness over 90° by 3.5%),
  - 60° (effective thickness -5.77 mm, increased thickness over 90° board by 15.5%),
  - 45° (effective thickness -7.07 mm, increased thickness over 90° board by 41.5%),
  - 30° (effective thickness -10 mm, increased thickness over 90° board by 100%),
- (Różyło, 2020, Ep. 1. and Ep. 2.).

In order to accelerate the performed calculations, the bullet model was designed as a non-deformable shell object, type Discrete rigid, base feature Shell, with a mesh type R3D4 (a 4-node 3-D bilinear rigid quadrilateral) composed of 700 finite elements. The bullet geometry is inspired by the 9 × 19 mm Parabellum pistol cartridge (Nieoczym & Drozd, 2021).

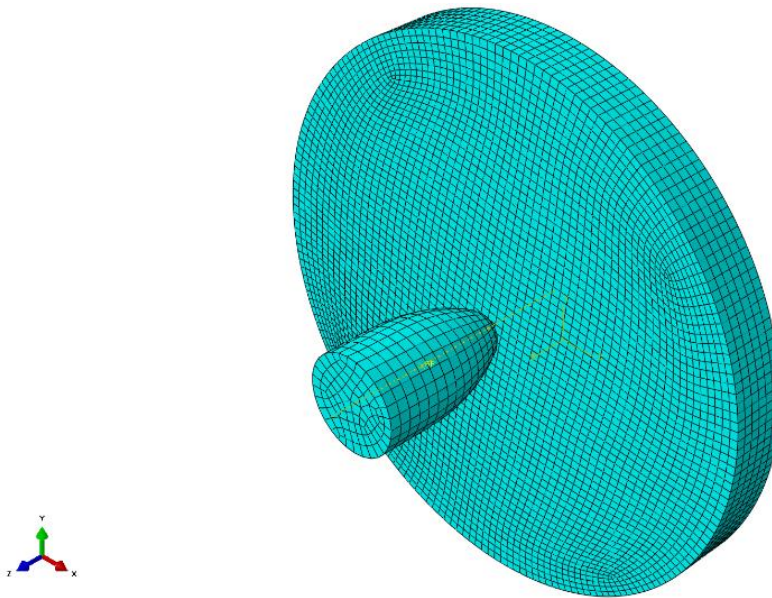


**Fig. 6. Composition and Mesh of the numerical model tested for 0° angle of attack**

The simulations were modelled as a dynamic analysis, taking into account geometric nonlinearities resulting from significant deformations. Due to the time-consuming nature of dynamic analyses, the duration of the analysis was limited, Time Period: 0.01, and in the model assembly the projectile was oriented at a short distance from the plate at the start of the analysis. Additionally, mass scaling was applied (Scale by factor = 600), this procedure significantly reduces the duration of the numerical analysis. The value of mass scaling, according to the principle of process acceleration, influences the course of the analysis and the results obtained. However, in the conducted analysis, the effect of the projectile angle of attack on the puncture is studied, which is not affected by the mass scaling phenomenon, as the analyses compared with each other were performed with the same scaling factor (Różyło, 2020a, 2020b).

### 3. RESULTS OF ANALYSIS

The highest stresses in the plate for all impact variants are observed on the projectile exit side in the axis to the direct point of contact of the projectile nose with the plate and in its vicinity. The occurrence of stress zones, i.e. places where the stress values are close to each other, was observed. During penetration of the plate by the projectile, propagation of stresses is observed, progressing from the point of impact, the zone of the highest stresses constantly increases until the hole, created as a result of the hit, reaches a value corresponding to or greater than the largest diameter of the projectile, then gradually the stresses reduce, producing the characteristic zones visible in the visualisations below. The maximum stress value was:  $S\text{-Misses}_{\max} = 550 \text{ MPa}$ .

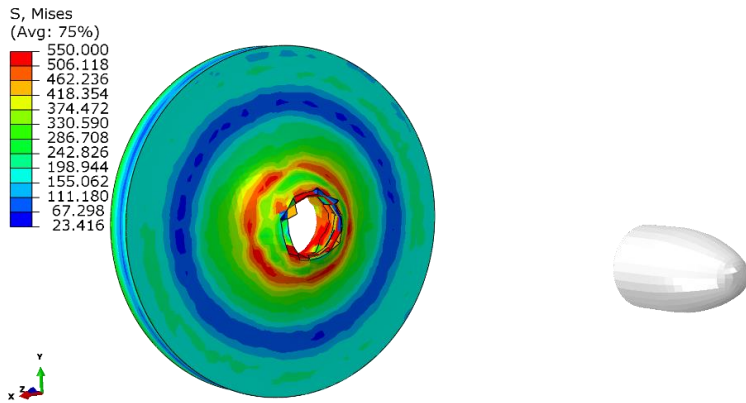
In the case of the  $90^\circ$  angle, the distribution of the values of the individual stresses assumes a characteristic shape close to circles, whose centre is the point of first contact of the projectile with the plate. The penetration surface, a fragment of the plate completely ruptured by the projectile, also assumes the shape of a circle. These stresses are characterised by a significant level of symmetry, relative to the individual planes. In Figure 7 it is possible to notice two zones of sudden decrease of stresses, the first one occurring near the centre of the plate, created between the zones of plasticised material, and the second one created near the place of creation of global deformations, this phenomenon can be noticed in all variants of simulations. In order to verify the statement concerning the second zone, it is necessary to conduct additional tests, for a larger diameter of the plate, due to the proximity of the outer edge of the plate to this zone.

For angles of  $75^\circ$ ,  $60^\circ$  and  $45^\circ$ , shows in a Figure 8–11, a deformation of the circles of the stress zones was observed in relation to the angle of attack of  $90^\circ$ . As the angle of attack increases, the distribution of these zones becomes less ordered, the stresses are less regularly distributed and take on increasingly distorted forms. Moreover, as the slope of the plate decreases, the zone of maximum stresses is closer to the point of impact of the projectile. For an angle of  $75^\circ$ , the stress zones take the shape of ellipses flattened along the horizontal plane. In the case of  $30^\circ$  projectile impact angle, it is not possible to isolate the stress zones due to the too small diameter of the tested plate; in order to observe their distribution, additional simulation must be carried out. The observed stress zones have irregular, strongly deformed shapes. The characteristic circles and ellipses found in the other variants were also not observed, but this finding cannot be unequivocally confirmed.

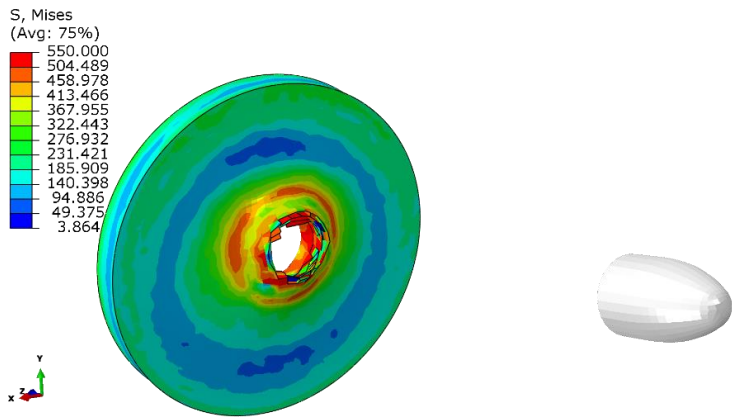
During the penetration of the plate by the projectile, observations were made regarding the maximum displacements in the plate, these were as follows:

- for an angle of  $90^\circ$ ,  $U_{\max} = 11.580 \text{ mm}$ ,
- for  $75^\circ$  angle,  $U_{\max} = 11.738 \text{ mm}$ ,
- for  $60^\circ$ ,  $U_{\max} = 10.211 \text{ mm}$ ,
- for  $45^\circ$ ,  $U_{\max} = 10.756 \text{ mm}$ ,
- for a  $30^\circ$  angle,  $U_{\max} = 10.328 \text{ mm}$ .

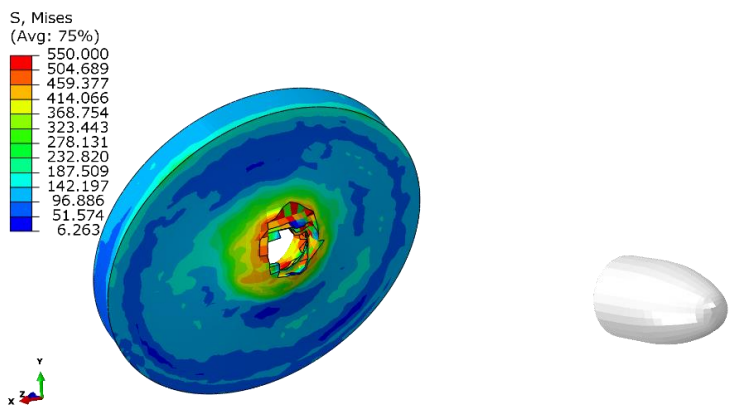
It was found that there was no dependence of the maximum deformation values on the projectile angle of attack. The highest deformation was obtained for an angle of  $75^\circ$ , while the lowest for an angle of  $60^\circ$ . In order to know the exact value of the displacement at which the maximum force for the puncture occurs, an additional analysis with a smaller calculation step must be carried out.



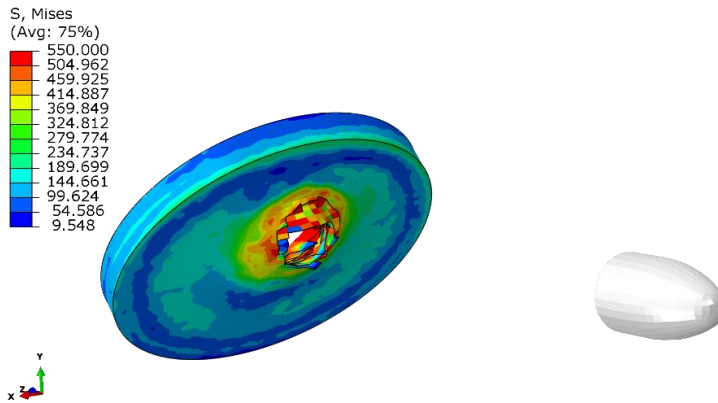
**Fig. 7. Visualisation of the projectile impact on the plate, angle of attack 90°**



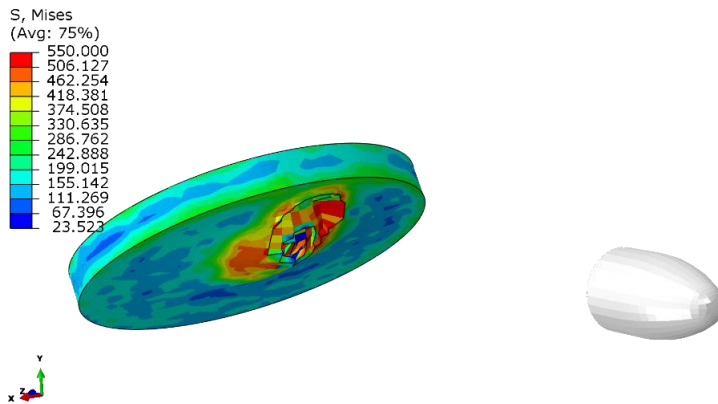
**Fig. 8. Visualisation of the projectile impact on the plate, angle of attack 75°**



**Fig. 9. Visualisation of the projectile impact on the plate, angle of attack 60°**



**Fig. 10. Visualisation of the projectile impact on the plate, angle of attack 45°**



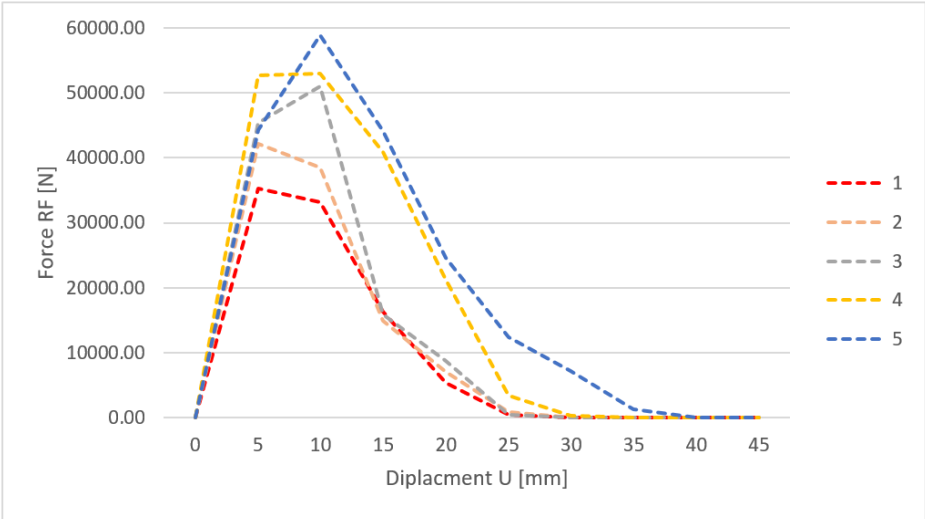
**Fig. 11. Visualisation of the projectile impact on the plate, angle of attack 30°**

Table 4 shows the values of forces obtained in the simulation against displacement. The highest value of the force needed for penetration was obtained for the angle of 30°, which is 58801.9 [N], while the lowest for the angle of 90°, which is 35211.2 [N]. Analysing the results, it is possible to notice an increase in the force required to penetrate the projectile with an increase in the angle of attack of the projectile. This is due to an increase in the effective thickness of the armour, resulting in a longer distance for the projectile to travel in the plate. For the first and second cases the maximum force value is observed for a displacement of 5 millimetres, for the other cases for a displacement value of 10 millimetres. The dependence of the maximum force on the displacement is shown in Figure 12. The change in the displacement value at which the maximum stress occurs is due to the fact that, as the angle of attack increases, the projectile travels a longer distance until the upper and lower surfaces of the nose contact the plate. Figure 13 shows the value of the maximum force required for penetration for all variants. The area of the surface in contact with the plate has a significant influence on the force needed for penetration and the value of the displacement. Analysing the graph, an almost linear tendency of the increase of the force required for

puncture was observed with the change of the slab inclination angle. Moreover, no proportionality of the increase in the force necessary for penetration with respect to the change in the effective thickness of the plate was observed. The lack of proportionality is due to a change in the area of the projectile in contact with the plate during penetration (Rodriguez-Millan et al., 2018).

**Tab. 4. Table of results obtained in the numerical analysis**

Number of simulation	1.		2.		3.		4.		5.	
Rake Angle	90°		75°		60°		45°		30°	
No.	U [mm]	RF [N]	U [mm]	RF [N]	U [mm]	RF [N]	U [mm]	RF [N]	U [mm]	RF [N]
1.	0	0.00	0	0	0	0	0	0	0	0
2.	5	35211.20	5	42105.4	5	45387.3	5	52729	5	44291
3.	10	33237.60	10	38472.1	10	51027.9	10	52963	10	58801.9
4.	15	16296.40	15	14929.1	15	15955.4	15	40900.9	15	44187.8
5.	20	5364.43	20	7135.66	20	8789.04	20	21304.9	20	24555.6
6.	25	495.19	25	939.91	25	481.784	25	3427.11	25	12404.3
7.	30	0.00	30	0	30	0	30	268.788	30	7271.49
8.	35	0.00	35	0	35	0	35	0	35	1364.85
9.	40	0.00	40	0	40	0	40	0	40	0



**Fig. 12. Diagram of the dependence of the force required for penetration on the angle of attack of the bullet**

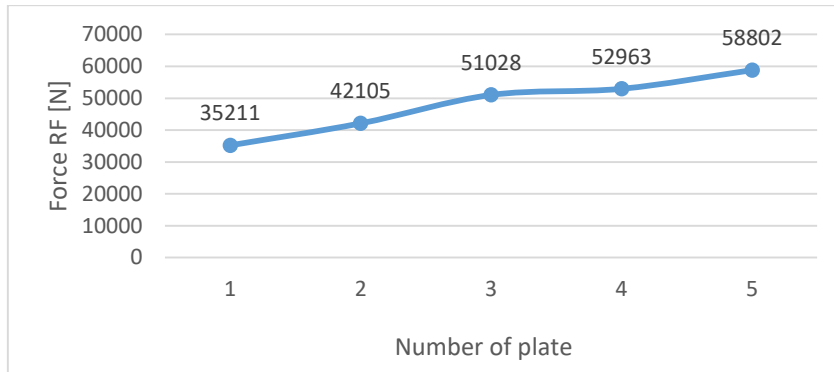


**Fig. 8. Maximum punching force value for individual plates**

#### 4. CONCLUSIONS

On the basis of the numerical analysis carried out in the Abaqus software, the following conclusions were drawn concerning the impact of the projectile on the steel plate.

1. Increasing the angle of attack of a projectile striking a plate, increases the force required to penetrate the plate. For a plate set at  $90^\circ$ , the force required to penetrate the plate increases by a value:

- 19.0% for a plate positioned at an angle of  $75^\circ$ ,
- 44.9% for a plate positioned at an angle of  $60^\circ$ ,
- 50.4% for a plate positioned at an angle of  $45^\circ$ ,
- 67% for a plate positioned at an angle of  $30^\circ$ .

2. The value of the force required for penetration increases approximately linearly with increasing angle of attack, and the largest increase in the energy required for penetration, relative to the previous position of the plate, is observed at an angle of  $60^\circ$  and is 25.9% relative to a plate positioned at  $75^\circ$ .

3. The elastic-plastic deformations were observed during the simulations, the highest value of plastic deformations is observed at the projectile impact site. The highest value of elastic deformation was observed on the plate wall opposite to the impact, in the vicinity of the projectile impact site.

4. For angles of  $75^\circ$ ,  $60^\circ$ ,  $45^\circ$  the increase in force required for penetration is greater than would be indicated by the percentage increase in armour thickness. The greatest differences were observed for the  $60^\circ$  angle, where the effective armour thickness increased by 15.5% and the force required for penetration increased by 44.9%, relative to the  $90^\circ$  plate.

In conclusion, the angle of attack of the plate is an important aspect influencing the strength of the plate when hit by a projectile. By increasing the angle of attack, safety can be improved without increasing the weight or changing the armour material. It should be borne in mind that the use of armour made up of inclined plates reduces the usable area of the vehicle. The values and percentage differences obtained are adequate for projectiles with a hemispherical tip. In order to assess the incremental force required to penetrate, as the angle of attack increases, for projectiles with other vertices (e.g. cylindrical, conical), additional numerical analysis must be carried out. However, it can be concluded that for all types of projectile tips, increasing the angle of attack increases the force required to penetrate a plate made of homogeneous isotropic material.

During the analysis of the results, the need for complementary analyses was identified. Such as:

- conducting analyses for a larger disc diameter, in order to know more precisely the stress distribution,
- carrying out the analysis for a smaller calculation step in order to know the exact displacement values for which the maximum stresses are obtained.

Due to the complexity of the topic related to the penetration of the plate by the projectile, additional analyses should be considered to complement the state of the art in ballistics, e.g. the effect of projectile velocity on the ability to penetrate a steel plate.

## REFERENCES

- Askariani, S. S., & Garivani, S. (2020). *More Details about Validation of Calibrated Parameters of Ductile Damage Model for A36 Steel Plates in Abaqus Software University of Bojnord*. University of Bojnord.
- Aufmann, F. (2020 March, 17). Stahl – und Panzer-Platten – Stalowe i pancerne plyty. <http://hauba.pl/stahl-und-panzer-platten-stalowe-i-pancerne-plyty>
- Bathe, K. J. (1996). *Finite Element Procedures*. Prentice Hall.
- Børvik, T., Hopperstada, O. S., Langsetha, M., & ArneMaloa, K. (2003). Effect of target thickness in blunt projectile penetration of Weldox 460 E steel plates. *International Journal of Impact Engineering*, 28(4), 413–464. [https://doi.org/10.1016/S0734-743X\(02\)00072-6](https://doi.org/10.1016/S0734-743X(02)00072-6)
- Budzyński, A. (2006). Krótki wstęp do zastosowania Metody Elementów Skończonych (MES) do numerycznych obliczeń inżynierskich. *Biuletyn „GM View”*, 5/2006.
- Czołg lekki BT-SV-2 „Turtle”. (n.d.). Retrieved March 16, 2020 from <https://pl.wv2facts.net/28359-light-tank-bt-sv-2-turtle.html>
- Fletcher, D. (2004). *British Mark I Tank 1916*. Osprey Publishing.
- Flis, L., & Sperski, M. (2011). Badania odporności balistycznej pancerzy ze stali 10GHMBA na ostrzał pociskami 12.7 mm. *Zeszyty naukowe Akademii Marynarki Wojennej*, 3(186), 27–42.
- Flis, L., & Sperski, M. (2012). Ocena wpływu kształtu wierzchołka pocisku na proces przebijania pancerzy stalowych. *Zeszyty naukowe Akademii Marynarki Wojennej*, 2(189), 29–44.
- Michulec, R., & Zientarzewski, M. (2006). *T-34 – Mityczna broń* (pp. 12–40). Wydawnictwo Armagedon.
- Nieoczym, A., & Drozd, K. (2021). Fractographic Assessment and FEM Energy Analysis of the Penetrability of a 6061-T Aluminum Ballistic Panel by a Fragment Simulating Projectile. *Advances in Science and Technology Research Journal*, 15(1), 50–57. <https://doi.org/10.12913/22998624/129951>
- Rodriguez-Millan, M., Garcia-Gonzalez, D., Rusinek, A., & Arias, A. (2018). Perforation mechanics of 2024 aluminium protective plates subjected to impact by different nose shapes of projectiles. *Thin-Walled Structures*, 123, 1–10.
- Różyło, P. (2020a) *Metoda elementów skończonych Praktyczne przykłady zagadnień statycznych i dynamicznych w programie Abaqus: Część 1*. Wydawnictwo Politechniki Lubelskiej.
- Różyło, P. (2020b) *Metoda elementów skończonych Praktyczne przykłady zagadnień statycznych i dynamicznych w programie Abaqus: Część 2*. Wydawnictwo Politechniki Lubelskiej.
- Senthil, K., Iqbal, M. A., Arindam, B., Mittal, R., & Gupta, N. K. (2018). Ballistic resistance of 2024 aluminium plates against hemispherical sphere and blunt nose projectiles. *Thin Walled Structures*, 126, 94–105.
- Simulia, D. (2017). *Abaqus 2017 documentation*. Dassault Systemes Waltham.
- Steel Construction Manual* (8th Edition, second revised edition). (1986). American Institute of Steel Construction.
- Tiwari, G., Iqbal, M. A., & Gupta, P. K. (2018). Energy absorption characteristics of thin aluminium plate against hemispherical nosed projectile impact. *Thin-Walled Structures*, 126, 246–257.
- Torecki, S., (1982). Przebijalność pocisku. *W 1000 słów o broni i balistyce* (pp. 177–179). Wydawnictwo Ministerstwa Obrony Narodowej.
- Tyutin, M. R., Botvina, L. R., & Petersen, T. B. (2020). Tensile damage evolution of structural steels with different structure. *Procedia Structural Integrity*, 28, 2148–2156. <https://doi.org/10.1016/j.prostr.2020.11.042>
- Wagner, R. H. N. (2021). *ABAQUS Tutorial: Damage for Ductile Metals – Material Model Explained – Ductile Damage*. Project: ABAQUS – Material Model Explained – Video Series.
- Wiśniewski, A., & Żurowski, W. (2002). *Amunicja i pancerze*. Politechnika Radomska.